# Average Link Rate Analysis over Finite Time Horizon in a Wireless Network

Sai Nisanth Bodepudi

Thesis submitted to the Faculty of the
Virginia Polytechnic Institute and State University
in partial fulfillment of the requirements for the degree of

Master of Science
in
Electrical Engineering

Allen B. MacKenzie, Co-chair
Harpreet S. Dhillon, Co-chair
Jeffrey H. Reed

February 17, 2017
Blacksburg, Virginia

Keywords: Ad hoc network, cellular network, Poisson point process, stochastic geometry, average rate

# Average Link Rate Analysis over Finite Time Horizon in a Wireless Network

Sai Nisanth Bodepudi

(ABSTRACT)

Instantaneous and ergodic rates are two of the most commonly used metrics to characterize throughput of wireless networks. Roughly speaking, the former characterizes the rate achievable in a given time slot, whereas the latter is useful in characterizing average rate achievable over a long time period. Clearly, the reality often lies somewhere in between these two extremes. Consequently, in this work, we define and characterize a more realistic *$N$-slot average rate* (achievable rate averaged over $N$ time slots). This $N$-slot average rate metric refines the popular notion of ergodic rate, which is defined under the assumption that a user experiences a complete ensemble of channel and interference conditions in the current session (not always realistic, especially for short-lived sessions).

The proposed metric is used to study the performance of typical nodes in both ad hoc and downlink cellular networks. The ad hoc network is modeled as a Poisson bipolar network with a fixed distance between each transmitter and its intended receiver. The cellular network is also modeled as a homogeneous Poisson point process. For both these setups, we use tools from stochastic geometry to derive the distribution of $N$-slot average rate in the following three cases: (i) rate across $N$ time slots is completely correlated, (ii) rate across $N$ time slots is independent and identically distributed, and (iii) rate across $N$ time slots is partially correlated. While the reality is close to third case, the exact characterization of the first two extreme cases exposes certain important design insights.

# Average Link Rate Analysis over Finite Time Horizon in a Wireless Network

Sai Nisanth Bodepudi

(GENERAL AUDIENCE ABSTRACT)

Choice of an appropriate metric is essential for accurate design and analysis of wireless networks. The two most popular metrics used to characterize data rate or throughput of wireless networks are instantaneous and ergodic rates. While instantaneous rate characterizes the throughput achievable in a given time slot, the ergodic rate characterizes the average achievable throughput over a long period of time. But often, the real-world scenarios fall in between these two extremes, where the network performance is to be characterized over a given finite number of time slots. Hence, we define and characterize a new suitable metric *$N$-slot average rate*, which is the achievable rate averaged over $N$ time slots.

Using this metric, we develop an analytical framework to study the performance of typical nodes in both ad hoc and downlink cellular networks. We model these networks using homogeneous Poisson point processes and characterize the $N$-slot average throughput using the tools of stochastic geometry. Accounting for the prominent cases of network mobility, we derive the distribution of $N$-slot average rate in the following three scenarios: rate is completely correlated across $N$ time slots, rate is independent and identically distributed across $N$ time slots, and rate is partially correlated across $N$ time slots. We studied the impact of various system parameters on our metric and also discussed key insights from our results.

# Acknowledgments

I extend my heartfelt gratitude to Dr. Harpreet Dhillon and Dr. Allen MacKenzie for guiding through all my research as well as grad school life. This thesis is the result of constant motivation and strong support you offered me throughout my Masters. Thanks to your your invaluable feedback and suggestions, these couple of years at Virginia Tech have been a great learning experience. You are my role models and I always draw inspiration from you. I sincerely thank you for being very empathetic and mentoring me to evolve my knowledge and skills.

I also earnestly thank Dr.Jeffrey Reed for agreeing to be a part of my thesis defense committee.

I thank my lab mates in Durham-470: Chiranjib, Karthik, Mustafa, Priyabrata, Shankar, Surabhi, Tapan and Vishnu for your support and all the fun times we had. I also thank Aditya, Deven, Raghu, Sai Dheeraj and other friends in Wireless@VT for being cheerful and supportive. And special thanks to Mehrnaz for mentoring and helping me since the beginning of my masters. I also thank my buddies Ashwitha, Bharadwaj, Harsha, Nikhitha, Rohith and Sai Ravi Kiran for being an integral part of my grad life.

A big thanks to my cousin Madhavi and brother-in-law Kiran for their love and support. Finally, I thank my parents who have been my strength and happiness. As ever, your support has played a key role during my masters, guiding me through difficult times.

# Contents

# List of Figures

# Chapter 1

# Introduction

Accurate modeling of the spatial topologies of wireless networks is indispensable for their realistic performance analysis. While the classical approaches to wireless network modeling usually relied on deterministic models (such as the popular grid-based models for cellular networks), more recent approaches are based on visualizing wireless network layouts as realizations of random spatial models. More concretely, the locations of wireless networks are endowed with appropriate distributions, which can often be tuned to match the real deployments, e.g., see [1–3]. In addition to being more realistic in capturing the increasing *irregularities* in the modern deployments, this approach is often more tractable owing to the additional randomness in the model, which can be exploited by using tools from stochastic geometry [4–6]. Interested readers are advised to refer to [7–11] for a pedagogical treatment of the topic and its applications to different types of wireless networks.

Owing to its simplicity and tractability, a homogeneous Poisson point process (PPP) is by far the most popular choice for modeling the locations of wireless nodes. A homogeneous PPP is identified with two important characteristics: In a given region $A$ of spatial area $\ell(A)$, the number of points $\Psi(A)$ in the region is Poisson distributed with mean $\lambda\ell(A)$, where $\ell(.)$ is the Lebesgue measure and $\lambda$ is the intensity of the homogeneous PPP. Furthermore, the number of points $\Psi(A_1), ...., \Psi(A_m)$ in $m$ disjoint regions $A_1, ..., A_m$ are independent. Please

refer to [4–6] for more details. This model will also form a key element of the analysis presented in this thesis. Please note that PPP-based models have already been applied to study almost every type of wireless network, including cellular networks [12], heterogeneous cellular networks [13], ad hoc networks [14], and cognitive radio networks [9].

After establishing a spatial model for a wireless network, the very next step is to select an appropriate performance metric. Examples of popularly used metrics include delay, throughput, and coverage probability. As will be discussed shortly, network throughput can be defined in several different ways. In this thesis, we are particularly interested in understanding the statistics of network throughput averaged over finite number of time slots. The motivation behind choosing this metric and its advantages over more classical throughput metrics will be discussed shortly.

The rest of this chapter is divided into three sections. The first section discusses two key metrics, coverage probability and throughput, and expands on the variants of the throughput or rate metric typically used in network analysis. The second section discusses the contributions of this thesis, and the third section presents the organization of the remaining chapters of this thesis.

## 1.1 Metrics to Characterize Network Performance

### 1.1.1 Coverage Probability

Coverage probability (also called success probability) is one of the most widely used metrics in the wireless communication literature. Roughly speaking, it characterizes the probability that the received signal at a chosen node is strong enough to enable successful reception. Concrete definition is provided next.

**Definition 1.** *(Coverage Probability) It is defined as the probability that the received signal to noise and interference ratio* (SINR) *or signal to interference ratio* (SIR) *at a particular*

*node exceeds a modulation and coding specific threshold $T$. In this thesis, it is denoted by $p_c$ and is mathematically defined as*

$$p_c = Pr\left(\text{SIR} > T\right). \tag{1.1}$$

From the above definition, it is clear that coverage probability is nothing but the complementary cumulative distribution function (CCDF) of SIR. Since SIR distribution is important for characterizing several other metrics, such as rate or throughput, as discussed next, coverage probability is an important component of several other metrics as well (in addition to being a useful stand alone metric). With this note, we now define rate or throughput next.

### 1.1.2 Rate or Throughput

Rate or throughput is another metric used to characterize network performance. Our research will primarily focus on a particular form of this metric, which will be defined shortly. The rate or throughput of a wireless link is often defined as the number of bits that can be transmitted from the transmitter to the receiver per second (and is expressed in terms of bits/sec). The sum of these link rates over all links in a network is sometimes called the *network rate*. There are two major notions of this metric, instantaneous rate and ergodic rate, which are popularly used for network performance analysis. Interested readers are referred to [14–19] for a representative subset of works focusing on characterizing different notions of throughput in wireless networks using tools from stochastic geometry.

#### Instantaneous Rate

Instantaneous rate represents the maximum achievable throughput in a given time slot. It is also known as *mean instantaneous channel capacity* in wireless standards [20].

**Definition 2.** *(Instantaneous Rate) For a channel with bandwidth $B$, the maximum achiev-*

*able throughput or rate (rate of information transmission without errors) over that channel in a given time slot is mathematically defined as*

$$R = B\left(\log_2(1 + \text{SINR})\right). \tag{1.2}$$

**Ergodic Rate**

Unlike instantaneous rate discussed above, ergodic rate characterizes the long-term average rate achievable over a wireless link. Roughly speaking, the average is over all possible realizations of the channel gain and interference power. It is formally defined next.

**Definition 3.** *(Ergodic Rate) The ergodic throughput or rate over a channel of bandwidth $B$ is the maximum achievable rate averaged over the complete ensemble and is mathematically defined as:*

$$R = \mathbb{E}\left[B\left(\log_2(1 + \text{SINR})\right)\right]. \tag{1.3}$$

*where $\mathbb{E}$ denotes the mathematical expectation.*

As discussed next, both these notions of rate have their limitations. In reality, neither instantaneous nor ergodic rate dictates the performance of wireless systems. In this thesis, we come up with a more realistic notion of rate that is briefly discussed next.

## 1.2 Contributions

Instantaneous rate and ergodic rate are applicable only to network analysis in instantaneous time and over a long time period, respectively. These metrics are not suitable to analyze network performance in given, finite time period (unless that finite time is on the order of the coherence time of the channel or smaller, in which case the instantaneous rate may be appropriate). Moreover, instantaneous rate does not always correspond to Quality of Service in wireless networks. For example, in case of Voice over Internet Protocol (VoIP),

the required average data rate is low, but it must be maintained consistently over the entire session time. This depends on the link quality over the VoIP session time and occasional variations in the packet transmission rate (could be due to network congestion) is permissible as long as the average rate is higher than a particular threshold. We address this challenge by defining a new metric called *N-slot Average Rate* which is the time average of rate over $N$ time slots. Using the tools of stochastic geometry, we develop an analytical framework for characterizing this new metric in bipolar ad hoc and downlink cellular networks.

For the characterization of this *N-slot Average Rate* metric, we need to first characterize the random variables involved, which are primarily fading gains and node locations. These random variables exhibit different properties in different scenarios. For example, in high mobility environments like highway traffic, users change their positions rapidly. Hence, the locations and channel fading gains can be considered independent and identically distributed (i.i.d.) from each user in each time slot. Whereas, in low mobility environments, like a coffee shop, movie theatre, or football stadium, the users tend to not move around much and their positions are almost constant for a relatively long time duration. Depending upon the channel coherence time and time slot duration, the fading in this case can be considered variable or constant in each time slot. Hence we characterized the network performance in all three network mobility scenarios - i.i.d. rate, completely correlated rate, and partially correlated rate. While the reality is often close to the third case, characterization and analysis of first two cases revealed significant insights which can be extended to the practical scenarios.

## 1.3 Organization

The technical contributions of this thesis are covered in Chapters 2 and 3. Chapter 2 develops an analytical framework for characterizing the average rate metric over finite time slots for a Poisson bipolar ad hoc network. Approximate analytical expressions for the distribution of

this metric under three cases discussed above were derived. Chapter 3 develops an analytical framework to characterize the same metric over finite time slots for a downlink cellular network with nodes distributed according to a PPP. Approximate analytical expressions are again derived for the proposed metric under the three cases discussed above. Finally, Chapter 4 summarizes the key contributions of this thesis and discusses some potential extensions of this research.

# Chapter 2

# Average Rate over Finite Time Slots in Ad Hoc Network

Mobile ad hoc networks are an important class of wireless networks that have drawn significant research attention. An illustration of an ad hoc network is presented in Figure 2.1. Stochastic geometry is a powerful tool to model these networks and mathematically study their performance characteristics [4, 5]. As discussed in the previous chapter already, the key idea in stochastic geometry-based network analysis is to model the transmitter and receiver node locations as point processes with given node densities and study their performance based on metrics such as coverage probability, delay, and throughput.

As noted already in the previous chapter, the main focus of this thesis is on characterizing the $N$-slot average rate, which in turn depends upon the SIR distribution experienced by the receiver of interest. As will be evident in the sequel, characterizing the exact distribution of SIR for the cases considered in this thesis is not straightforward. As a result, we will be deriving approximate expressions under the so called *dominant-interferer* (DI) approach [19, 21–24]. This approach is based on the fact that the aggregate interference seen at a receiver is dominated by a few near-by interferers. As demonstrated recently in [21–24], this approach leads to tractable approximate expressions, which when plotted are almost

Figure 2.1: Figure depicting ad hoc connections between the mobiles in a MANET

indistinguishable from the true results. We will also present such numerical comparisons for the proposed metric in this thesis.

In this chapter we consider a bipolar mobile ad hoc network, also referred to as bipolar MANET, where the locations of transmitters are modeled by a homogenous PPP with a given node density and each associated receiver is at certain fixed distance from its transmitter [5]. This model is also called the dumbbell model and has been popularly used to study ad hoc networks with tractable results, see [25–28] for a small subset. We evaluate the CCDF of $N$-slot average rate metric, which is the probability that $N$-slot average rate of the network is greater than a threshold.

## 2.1 Spatial Aloha in a Poisson Ad Hoc Network

### 2.1.1 System Model

As noted above, the locations of the transmitter and receivers are modeled according to a Poisson bipolar model, in which the transmitter nodes are distributed on a 2-dimensional

plane according to a homogeneous PPP, and each associated receiver node is located at a fixed distance $r$, called the serving distance, from the associated transmitter. We consider Aloha medium access control with slotted time. The transmitter locations form a homogenous PPP with density $\lambda$ in every time slot [5]. We denote the medium access probability of a typical link by $p'$. The interfering nodes transmit and mute with probabilities $p$ and $1-p$, respectively. The locations of the transmitting nodes in time slot $k$ are denoted by the homogeneous PPP $\tilde{\Phi}_k$. Owing to the stationarity of this setup, the analysis will be performed for a typical link with the receiver located at the origin and its designated transmitter at distance $r$ from the origin.

We model the path loss for a wireless link between a transmitter located at $x$ and a receiver located at $y$ on a plane as: $l(x,y) = \|x-y\|^{-\alpha}$ where $\alpha > 2$ is the pathloss exponent, and $\|x-y\|$ represents the Euclidean distance between points $x$ and $y$. In our subsequent analysis, we denote the pathloss function by $l(\|x\|) = \|x\|^{-\alpha}$ where $\alpha > 2$ is the pathloss exponent, and the argument $\|x\|$ represents the Euclidean distance between points $x$ and the origin. We assume Rayleigh fading channels and that the fading gains are i.i.d. across all communication links in all time slots. The fading gain for a wireless link between transmitter node at $X_{j_{\tilde{\Phi}_k}}$ and receiver node at origin in time slot $k$ is represented by $h_{j,k} \sim \exp(1)$. Without loss of generality, we assume that transmit powers of all transmitting nodes are unity in all time slots. We denote the aggregate interference at the origin in time slot $k$ by $I_{\tilde{\Phi}_k}$.

### 2.1.2 Three Setup of Interest

As discussed earlier, based on the network mobility scenarios, we have the following three cases:

**Completely Correlated Rate**

In this case, nodes are immobile across the set of time slots considered, and the values assumed by each of the fading random variables remain constant across the set of time slots. Hence, there is complete correlation in interference and thereby in rate across the time slots in this scenario.

**Independent and Identically Distributed (i.i.d.) Rate**

In this case, we assume that mobility is high, so that the location of the interfering nodes (i.e. the PPP $\tilde{\Phi}_k$) in different time slots is i.i.d. In other words, we assume that the receiver of interest experiences independent realizations of interferers over all time slots. Also, the channel fading gain is i.i.d. across the time slots, and thus the interference $I_{\tilde{\Phi}_k}$ is i.i.d. across time slots. Hence, the rate in each individual time slot, denoted by $R_k$ is i.i.d. in this scenario.

**Partially Correlated Rate**

This case lies in between the two extreme cases discussed above. Here, the nodes are immobile in the time slots considered, but the fading random variables are i.i.d. across those time slots. Here, the partial correlation refers to the complete correlation in node locations combined with the i.i.d. realizations of the fading random variables.

## 2.2 $N$-slot Average Rate Distribution

Before deriving the average rate distribution, we first study the coverage probability.

### 2.2.1 Coverage Probability

Assuming an interference-limited network, a transmitter node is said to cover its associated receiver if the SIR is greater than a threshold ($T$) at the receiver. For a typical link with its receiver at origin, the SIR in time slot $k$ is given as:

$$\mathrm{SIR}_k := \frac{h_{0,k} l(\|X_{0_{\tilde{\Phi}_k}}\|)}{I_{\tilde{\Phi}_k}} \tag{2.1}$$

where the typical receiver is at origin and $I_{\tilde{\Phi}_k}$ is given by:

$$I_{\tilde{\Phi}_k} = \sum_{X_{j_{\tilde{\Phi}_k}} \in \tilde{\Phi}_k, j \neq 0} h_{j,k} l(\|X_{j_{\tilde{\Phi}_k}}\|). \tag{2.2}$$

**Lemma 1.** Under Rayleigh Fading, the coverage probability of a typical node ($p_c(r, p, \lambda, T)$) is

$$p_c(r, p, \lambda, T) = \exp\{-2\pi\lambda p r^2 T^{2/\alpha} K(\alpha)\} \tag{2.3}$$

where $K(\alpha) = \frac{1}{\alpha}\Gamma(\frac{2}{\alpha})\Gamma(1 - \frac{2}{\alpha})$. This is a very well-known result. See for instance [5] for the proof.

We use this result to derive an expression for the distribution of average rate.

### 2.2.2 Distribution of Average Rate

In our network model, the rate or throughput of a node in bits/sec/Hz in a given time slot $k$ is given by:

$$R_k = p' \log_2(1 + \mathrm{SIR}_k), k \geq 1 \tag{2.4}$$

where $\mathrm{SIR}_k$ is the signal-to-interference ratio of the typical node in a particular time slot $k$ and is given by (2.1). We now define our metric, the $N$-slot time average of throughput as follows:

$$\tilde{R} = \frac{\sum_{k=1}^{N} R_k}{N} \tag{2.5}$$

where $N$ is the number of time slots over which the rate is averaged. Having defined $\tilde{R}$, we denote the probability that $N$-slot average rate is larger than some threshold $T$ (bits/sec/Hz) i.e. $Pr(\tilde{R} > T)$ by $(P_R)$, which is given by

$$P_R = Pr\left(\frac{\sum_{k=1}^{N} R_k}{N} > T\right) \tag{2.6}$$

$$= Pr\left(\frac{\sum_{k=1}^{N} p' \log_2\left(1 + \frac{h_{0,k} l(r)}{\sum_{X_{j_{\tilde{\Phi}_k}} \in \tilde{\Phi}_k, j \neq 0} h_{j,k} l(\|X_{j_{\tilde{\Phi}_k}}\|)}\right)}{N} > T\right). \tag{2.7}$$

For this setup, we derive the distribution of the $N$-slot average rate in the three cases.

**Completely Correlated Rate**

When the rate achievable across different time slots is the same, say $R_k = R, \forall k$, the CCDF of $N$-slot average rate, $P_R$ reduces to CCDF of rate in a single time slot which is derived as follows:

$$P_R : = Pr\left(R > T\right) \tag{2.8}$$

$$= Pr\left(R_k > T\right) \tag{2.9}$$

$$= Pr\left(p' \log_2(1 + \mathrm{SIR}) > T\right) \tag{2.10}$$

$$= Pr\left(\mathrm{SIR} > 2^{T/p'} - 1\right) \tag{2.11}$$

$$= \exp\left(-2\pi\lambda p r^2 (2^{T/p'} - 1)^{2/\alpha} K(\alpha)\right) \tag{2.12}$$

the last equation follows from (2.3).

**The i.i.d. Rate**

The expression for the i.i.d. rate case is given as follows:

$$P_R = Pr\left(\frac{\sum_{k=1}^{N} p' \log_2\left(1+\frac{h_{0,k}l(r)}{I_{\tilde{\Phi}_k}}\right)}{N} > T\right) \tag{2.13}$$

where $I_{\tilde{\Phi}_k}$ and $h_{0,k}$ are i.i.d. across time slots $k$, and hence $R_k$ are i.i.d.

While it is, in principle, possible to derive the exact expression for $P_R$ by first calculating the characteristic function of individual rates $R_k$ and then multiplying these to compute the characteristic function of $N$-slot average rate $\tilde{R}$, which can eventually be inverted to compute the distribution of $\tilde{R}$. This inversion step is usually not very tractable. Therefore, in order to maintain tractability, we approximate $P_R$ by carefully applying Central Limit Theorem (CLT), as explained next.

In order to apply CLT, we first evaluate the mean and second moment of $R_k$ (denoted by $\mu_{R_k}$ and $M_{R_k}$, respectively), and thereby variance of $\tilde{R}$ (denoted by $\sigma^2_{\tilde{R}}$). These results follow from the application of standard tools from stochastic geometry [5]. Since $R_k$ are i.i.d. random variables, the mean of $\tilde{R}$ is: $E[\tilde{R}] = E[R_k]$. Since, rate is a non-negative random variable, mean of $R_k$ can be written as:

$$\mu_{R_k} = \mathbb{E}[R_k] = \int_0^\infty Pr\left(p' \log_2(1+\mathrm{SIR}_k) > x\right) \mathrm{d}x \tag{2.14}$$

$$= \int_0^\infty \exp\left(-2\pi\lambda p r^2 (2^{x/p'}-1)^{2/\alpha} K(\alpha)\right) \mathrm{d}x. \tag{2.15}$$

By using the variable transformation: $y = (2^{x/p'} - 1)$, we derive the expression for mean $(\mu_{\tilde{R}})$ of $\tilde{R}$:

$$\mu_{\tilde{R}} = \mu_{R_k} = \frac{p'}{\ln 2} \int_0^\infty \frac{\exp(-Cy^{2/\alpha})}{1+y} \mathrm{d}y \tag{2.16}$$

where $C = 2\pi\lambda p r^2 K(\alpha)$ is a constant.

Similarly, the second moment of each individual $R_k$ is given by:

$$E[R_k^2] = \int_0^\infty Pr\left((p' \log_2(1+\mathrm{SIR}_k))^2 > x\right) \mathrm{d}x \tag{2.17}$$

$$= \int_0^\infty Pr\left(p' \log_2(1+\mathrm{SIR}_k) > \sqrt{x}\right) \mathrm{d}x \tag{2.18}$$

$$= \int_0^\infty Pr\left(\mathrm{SIR}_k > 2^{\sqrt{x}/p'} - 1\right) \mathrm{d}x \tag{2.19}$$

$$= \int_0^\infty \exp\left(-2\pi\lambda p r^2 \left(2^{\sqrt{x}/p'} - 1\right)^{2/\alpha} K(\alpha)\right) \mathrm{d}x \tag{2.20}$$

the above equation follows from (2.3). By using the variable transformation: $y = (2^{\sqrt{x}/p'} - 1)$, we derive the expression for $M_{R_k}$:

$$M_{R_k} = \frac{2p'^2}{\ln 2} \int_0^\infty \frac{\log_2(1+y)\exp(-Cy^{2/\alpha})}{1+y} dy \tag{2.21}$$

where $C = 2\pi\lambda p r^2 K(\alpha)$.

Since $R_k$ are i.i.d., variance of $\tilde{R}$ is calculated as follows:

$$\sigma_{\tilde{R}}^2 = \frac{M_{R_k} - \mu_{\tilde{R}}^2}{N}. \tag{2.22}$$

Using the mean and variance, we derive the desired CCDF of $\tilde{R}$ ($P_R$) as follows:

$$P_R = \varphi\left(\frac{x - (\mu_{\tilde{R}})}{\sqrt{\frac{M_{R_k} - (\mu_{\tilde{R}})^2}{N}}}\right) = \varphi\left(\frac{x - (\mu_{\tilde{R}})}{\sqrt{\sigma_{\tilde{R}}^2}}\right) \tag{2.23}$$

where the function $\varphi$ is the CCDF of a standard Normal random variable. It should be noted that this expression is an approximation due to the application of CLT.

**Partially Correlated Rate**

The expression for $N$-slot average rate distribution in this case is given by:

$$P_R = Pr\left( \frac{\sum_{k=1}^{N} p' \log_2\left(1 + \frac{h_{0,k} l(r)}{I_{\tilde{\Phi},k}}\right)}{N} > T \right) \tag{2.24}$$

where the locations of transmitter nodes remains constant ($\tilde{\Phi}$) across time slots $k$, but, the fading gain of each link is i.i.d. across the $N$ time slots. Since the distribution of node locations is the same for all time slots, we use $I_{\tilde{\Phi},k}$ (instead of $I_{\tilde{\Phi}_k}$) to denote the interference term in partially correlated rate.

To evaluate the mathematical expression for $P_R$, we approximate the aggregate interference by the interference from the closest interferer, which we term the dominant interferer. After taking the DI approximation and conditioning on the location of the DI, the approximated individual rates $R'_k$ are i.i.d. (because the only sources of randomness now are the channel gains, which are assumed to be i.i.d. across time slots) and we can hence apply the central limit theorem to approximate the CCDF, as we did in the prior case.

An expression for the CCDF of rate derived using the DI approximation is as follows:

$$P_R = Pr\left( \frac{\sum_{k=1}^{N} p' \log_2\left(1 + \frac{h_{0,k} l(r)}{h_k l(D)}\right)}{N} > T \right) \tag{2.25}$$

where $l(D) = D^{-\alpha}$ represents the path loss function for the DI, $h_k$ represents the channel gain for DI link and the random variable $D$ denotes the Euclidean distance of the DI from origin.

Once we condition on the random variable $D$, each individual rate $R'_k$ becomes identical and independent and then we used the CLT approximation as done earlier. After deriving

the conditional CCDF of rate, we decondition it with respect to the DI distribution to get the desired distribution of $N$-slot average rate. We evaluate the conditional mean and conditional variance of $\tilde{R}$ as follows:

The expression for DI-approximated rate in the correlated case ${R'}_k$ is given by:

$$ {R'}_k = p' \log_2 \left(1 + \frac{h_{0,k} r^{-\alpha}}{h_k D^{-\alpha}}\right). \tag{2.26} $$

Now, we derive the conditional CDF of SIR (conditioned on $D = d_1$):

$$ \begin{aligned} F_{\mathrm{SIR}' \,|\, d_1}(x) \quad &= Pr\left(\frac{h_{0,k} r^{-\alpha}}{h_k D^{-\alpha}} \leq x \,|\, D = d_1\right) && (2.27)\\ &= \mathbb{E}_{h_k}\left[Pr\left(h_{0,k} \leq \frac{x h_k {d_1}^{-\alpha}}{r^{-\alpha}} \,|\, d_1, h_k\right)\right] && (2.28)\\ &= \mathbb{E}_{h_k}\left[1 - \exp\left\{-\left(\frac{x h_k {d_1}^{-\alpha}}{r^{-\alpha}}\right)\right\} \,|\, d_1\right] && (2.29)\\ &= 1 - \int_0^\infty \exp\left\{-\left(\frac{x h_k {d_1}^{-\alpha} + h_k r^{-\alpha}}{r^{-\alpha}}\right)\right\} \mathrm{d}h_k && (2.30)\\ &= 1 - \frac{1}{x\left(\frac{{d_1}^{-\alpha}}{r^{-\alpha}}\right) + 1}. && (2.31) \end{aligned} $$

Using this result, we now compute the conditional rate in time-slot $k$ as follows:

$$ Pr\left({R'}_k \leq x \,|\, d_1\right) = Pr\left(\mathrm{SIR}' \leq (2^{x/p'} - 1) \,|\, d_1\right) = F_{\mathrm{SIR}' \,|\, d_1}(2^{(x/p')} - 1). \tag{2.32} $$

$$ Pr\left({R'}_k > x \,|\, d_1\right) = \frac{\left(\frac{r}{d_1}\right)^{-\alpha}}{2^{(x/p')} + \left(\frac{r}{d_1}\right)^{-\alpha} - 1}. \tag{2.33} $$

As was the case earlier, we use this conditional CCDF to compute the conditional mean and second moment of $N$-slot average rate, which will be useful in computing its distribution using CLT.

$$ \mu_{\tilde{R}|D=d_1} \quad = E\left[\tilde{R} \,|D = d_1\right] \tag{2.34} $$

$$= E\left[R'_k | D = d_1\right] \tag{2.35}$$

$$= \int_0^\infty Pr\left(R'_k > x \,|D = d_1\right) \mathrm{d}x \tag{2.36}$$

$$= \int_0^\infty \frac{\left(\frac{r}{d_1}\right)^{-\alpha}}{2^{(x/p')} + \left(\frac{r}{d_1}\right)^{-\alpha} - 1} \mathrm{d}x. \tag{2.37}$$

Using variable transformations: $\left(\frac{r}{d_1}\right)^{-\alpha} - 1 = M$ and $2^{(x/p')} = e^y$,

$$\mu_{\tilde{R}|D=d_1} = \frac{p'}{\ln(2)} \left(\frac{M+1}{M}\right) \int_0^\infty \left(1 - \frac{e^y}{M + e^y}\right) \mathrm{d}y \tag{2.38}$$

$$= \frac{\alpha\, r^{-\alpha}\, p'}{\ln(2)} \left(\frac{\ln d_1 - \ln\, r}{r^{-\alpha} - d_1^{-\alpha}}\right). \tag{2.39}$$

We follow similar procedure as above to derive the expression for second moment of rate, but, an exact closed-form expression is not possible in this case as it involves the integral of complex polylogarithmic functions.

$$M_{R'_k|D=d_1} = E\left[{R'_k}^2 | D = d_1\right] \tag{2.40}$$

$$= \int_0^\infty Pr\left({R'_k}^2 > x \,|D = d_1\right) \mathrm{d}x \tag{2.41}$$

$$= \int_0^\infty Pr\left(R'_k > \sqrt{x} \,|D = d_1\right) \mathrm{d}x \tag{2.42}$$

$$= \int_0^\infty \frac{\left(\frac{r}{d_1}\right)^{-\alpha}}{2^{\left(\sqrt{x}/p'\right)} + \left(\frac{r}{d_1}\right)^{-\alpha} - 1} \mathrm{d}x. \tag{2.43}$$

We evaluate the conditional variance of $\tilde{R}$ using (2.22) and derive the conditional CCDF as follows. Knowing the mean and variance of a normal distribution, its CCDF ($\bar{F}$)

is given by (2.23). The pdf of the distance of DI from origin is given as follows [29]:

$$f_D(x) = 2p\lambda\pi x \exp\left(-p\lambda\pi x^2\right). \tag{2.44}$$

Here, we use density $p\lambda$ to account for the thinning of the original PPP of interfering nodes due to their medium access probability ($p$).

Now we get the desired CCDF of $\tilde{R}$ by deconditioning it with respect to the DI as follows:

$$P_{\tilde{R}} = \int_0^\infty \bar{F}(\tilde{R}|D = d_1) f_D(d_1)\, \mathrm{d}d_1. \tag{2.45}$$

$$P_{\tilde{R}} = \int_0^\infty \varphi\left(\frac{x - \left(\mu_{\tilde{R}|D=d_1}\right)}{\sqrt{\frac{M_{R'_k|D=d_1} - \left(\mu_{\tilde{R}|D=d_1}\right)^2}{N}}}\right) f_D(d_1)\, \mathrm{d}d_1. \tag{2.46}$$

This DI approximation doesn't yield tight results as we ignored the interference from rest of the interferers (non-dominant interferers) (see Figure 2.6).

A more accurate approach to evaluate the mathematical expression for $P_R$ is to approximate the interference by the sum of interference from DI and mean of the interference from rest of the interferers (the non-dominant interferers) conditioned on the location of the DI.

**Assumption 1.** We assume that conditional on the distance to DI, $D = d_1$, the aggregate interference from the rest of the network can be accurately approximated by its conditional mean (conditioned on $d_1$). This assumption will be numerically validated later in this chapter.

This technique gives a simple and accurate approximation in our analysis as shown later in the numerical results section.
Interference in the partially correlated rate case is given by:

$$I_{\tilde{\Phi},k} = \sum_{X_j \in \tilde{\Phi},\, j \neq 0} h_{j,k} l(\|X_j\|). \tag{2.47}$$

Representing the interference from DI as $I_{DI}$ and its distance from the origin $D = \|X_1\|$ and the interference from the rest as $I_{nDI}$, we approximate the above interference by the sum of $I_{DI}$ and $\mathbb{E}\left[I_{nDI} \middle| D = d_1\right]$ and call the resulting approximation of total interference $\hat{I}_{\tilde{\Phi},k}$:

$$\hat{I}_{\tilde{\Phi},k} = h_{1,k} {d_1}^{-\alpha} + \mathbb{E}\left[\sum_{X_j \in \tilde{\Phi},\, j \neq \{0,1\}} h_{j,k} l(\|X_j\|) \,|\, d_1\right]. \tag{2.48}$$

The conditional expectation of $I_{nDI}$ is:

$$\mathbb{E}\left[I_{nDI} \middle| d_1\right] = \frac{2p\pi\lambda}{\alpha - 2} {d_1}^{2-\alpha} \tag{2.49}$$

for $\alpha > 2$; otherwise unbounded [21]. Hence, the total approximated interference is:

$$\hat{I}_{\tilde{\Phi},k} = h_{1,k} {d_1}^{-\alpha} + \frac{2p\pi\lambda}{\alpha - 2} {d_1}^{2-\alpha}. \tag{2.50}$$

By conditioning on the DI location, after taking the above approximations, the individual interferences and hence the individual rates $R_k$ become i.i.d. because the only random variables in the rate expression are those of fading (which are i.i.d.). Hence, now we can apply the CLT as we did in the previous case. In order to do that, we evaluate the conditional mean and conditional variance of $\tilde{R}$ as follows:

The expression for individual rate in the partially correlated case is given by:

$$\hat{R}_k = p' \log_2\left(1 + \frac{h_{0,k} r^{-\alpha}}{\hat{I}_{\tilde{\Phi},k}}\right) \tag{2.51}$$

$$= p' \log_2\left(1 + \frac{h_{0,k} r^{-\alpha}}{h_{1,k} {d_1}^{-\alpha} + V(d_1)}\right) \tag{2.52}$$

where $V(d_1) = \left(\frac{2p\pi\lambda}{\alpha - 2} {d_1}^{2-\alpha}\right)$.

The conditional CDF of interference term (conditioned on $d_1$) can now be expressed as:

$$Pr\left(\hat{I}_{\tilde{\Phi},k} \leq x \,|\, d_1\right) = Pr\left(h_{1,k} {d_1}^{-\alpha} + V(d_1) \leq x \,|\, d_1\right) \tag{2.53}$$

$$= Pr\left(h_{1,k} \leq \left(\frac{x - V(d_1)}{{d_1}^{-\alpha}}\right) \mid d_1\right) \tag{2.54}$$

$$= 1 - \exp\left\{-\left(\frac{x - V(d_1)}{{d_1}^{-\alpha}}\right)\right\},\ x > V(d_1); else\ 0. \tag{2.55}$$

$$f_{\hat{I}_{\tilde{\Phi},k}}(x \mid d_1) = \frac{\mathrm{d}}{\mathrm{d}x}\left(Pr\left(\hat{I}_{\tilde{\Phi},k} \leq x \mid d_1\right)\right) \tag{2.56}$$

$$= \left(\frac{1}{{d_1}^{-\alpha}}\right)\exp\left\{-\left(\frac{x - V(d_1)}{{d_1}^{-\alpha}}\right)\right\}. \tag{2.57}$$

The conditional CDF of SIR is derived as follows:

$$F_{\mathrm{SIR} \mid d_1}(x) = Pr\left(\frac{h_{0,k} r^{-\alpha}}{\hat{I}_{\tilde{\Phi},k}} \leq x \mid d_1\right) \tag{2.58}$$

$$= \mathbb{E}_{\hat{I}_{\tilde{\Phi},k}}\left[Pr\left(h_{0,k} \leq \frac{x\hat{I}_{\tilde{\Phi},k}}{r^{-\alpha}} \mid \hat{I}_{\tilde{\Phi},k}, d_1\right)\right] \tag{2.59}$$

$$= \mathbb{E}_{\hat{I}_{\tilde{\Phi},k}}\left[1 - \exp\left(-\left(\frac{x\hat{I}_{\tilde{\Phi},k}}{r^{-\alpha}}\right)\right) \mid d_1\right] \tag{2.60}$$

$$= 1 - \int_V^{\infty} \frac{\exp\left(\frac{-x\hat{I}_{\tilde{\Phi},k}}{r^{-\alpha}} + \frac{V(d_1) - \hat{I}_{\tilde{\Phi},k}}{{d_1}^{-\alpha}}\right)}{{d_1}^{-\alpha}} \mathrm{d}\hat{I}_{\tilde{\Phi},k} \tag{2.61}$$

$$= 1 - \frac{\exp\left\{-\left(\frac{2p\pi\lambda\, {d_1}^{2-\alpha}}{(\alpha-2)\, r^{-\alpha}}\right)x\right\}}{x\left(\frac{{d_1}^{-\alpha}}{r^{-\alpha}}\right) + 1}. \tag{2.62}$$

Now, using this we can compute:

$$Pr\left(\hat{R}_k \leq x \mid d_1\right) = Pr\left(\mathrm{SIR} \leq (2^{x/p'} - 1) \mid d_1\right) \tag{2.63}$$

$$= 1 - \frac{\exp\left\{-\left(\frac{2p\pi\lambda\, {d_1}^{2-\alpha}}{(\alpha-2)\, r^{-\alpha}}\right)(2^{x/p'} - 1)\right\}}{(2^{x/p'} - 1)\left(\frac{{d_1}^{-\alpha}}{r^{-\alpha}}\right) + 1}. \tag{2.64}$$

From this the conditional CCDF can be computed as:

$$Pr\left(\hat{R}_k > x \mid d_1\right) = \frac{\exp\left\{-\left(2^{x/p'} - 1\right)\frac{2p\pi\lambda r^2}{\alpha - 2}\left(\frac{d_1}{r}\right)^{2-\alpha}\right\}}{\left(2^{x/p'} - 1\right)\left(\frac{d_1}{r}\right)^{-\alpha} + 1}. \tag{2.65}$$

In order to apply CLT, we need the first and second moment, which are computed next:

$$\mu_{\hat{R}_k|D=d_1} = \int_0^\infty \frac{\exp\left\{-\left(2^{x/p'}-1\right)\frac{2p\pi\lambda r^2}{\alpha-2}\left(\frac{d_1}{r}\right)^{2-\alpha}\right\}}{\left(2^{x/p'}-1\right)\left(\frac{d_1}{r}\right)^{-\alpha}+1}\,\mathrm{d}x. \tag{2.66}$$

$$M_{\hat{R}_k|D=d_1} = \int_0^\infty \frac{\exp\left\{\left(1-2^{\sqrt{x}/p'}\right)\frac{2p\pi\lambda r^2}{\alpha-2}\left(\frac{d_1}{r}\right)^{2-\alpha}\right\}}{\left(2^{\sqrt{x}/p'}-1\right)\left(\frac{d_1}{r}\right)^{-\alpha}+1}\mathrm{d}x. \tag{2.67}$$

We then evaluate the conditional variance of $\tilde{R}$ using (2.22) and derive the conditional CCDF of rate $\bar{F}(\tilde{R}|D=d_1)$ using (2.23). Now we derive the desired CCDF of average rate (represented as $\widehat{P}_R$) by deconditioning with respect to the DI distance ($d_1$) as follows:

$$\widehat{P}_R = \int_0^\infty \bar{F}(\tilde{R}|D=d_1) f_D(d_1)\,\mathrm{d}d_1 \tag{2.68}$$

$$= \int_0^\infty \varphi\left(\frac{x-\left(\mu_{\tilde{R}|D=d_1}\right)}{\sqrt{\frac{M_{\hat{R}_k|D=d_1}-\left(\mu_{\tilde{R}|D=d_1}\right)^2}{N}}}\right) f_D(d_1)\,\mathrm{d}d_1 \tag{2.69}$$

where the function $\varphi$ is the CCDF of a standard Normal random variable.

## 2.3 Results and Discussion

In this section, we present the numerical results and demonstrate the accuracy of the approximate expressions derived for various cases. As expected, the probability $P_R$ increases with decrease in density of interfering transmitter nodes, increase in the path-loss exponent, decrease in medium access probability of interfering nodes, increase in medium access probability of typical node, and decrease in the serving distance.

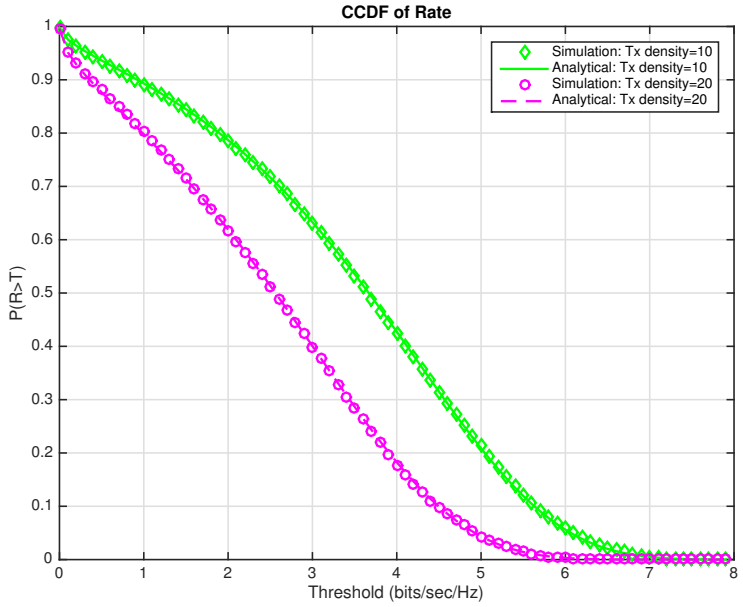


Figure 2.2: Dependence of rate on transmitter nodes density - Simulation vs Analysis. $P_R$ decreases with increase in $\lambda$.

### 2.3.1 Dependence on Nodal Density $\lambda$

When the density of interfering nodes increases, the interference at the receiver of the typical node increases, while the power received from the associated transmitter remains the same. Thus, the SIR and $P_R$ decrease. This effect can be observed in Figure 2.2.

### 2.3.2 Dependence on Path-loss Exponent $\alpha$

When the path-loss exponent increases, the signal power at the typical receiver from its associated transmitter decreases. However, the signal powers from every interfering node also decrease. Overall, we observe that the interference decreases more than the signal power and hence SIR increases. Figure 2.3 shows this effect.

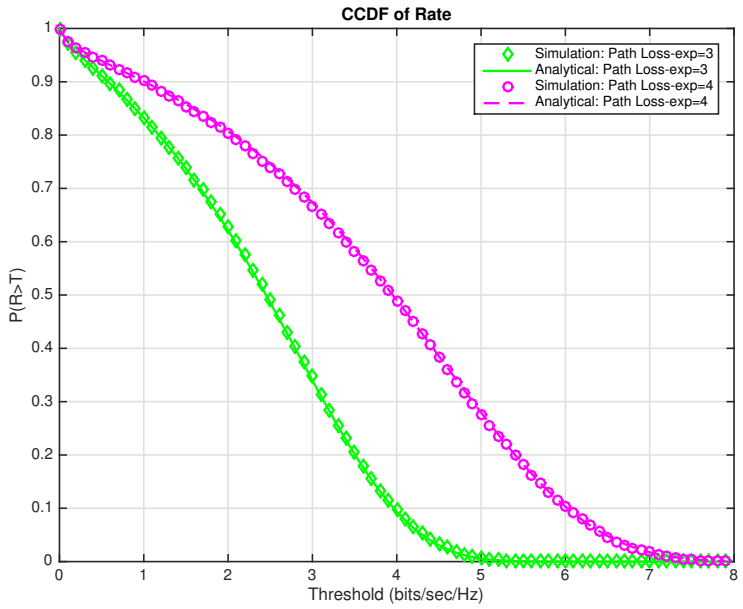


Figure 2.3: Dependence of rate on path loss exponent - Simulation vs Analysis. $P_R$ increases with increase in $\alpha$.

### 2.3.3 Dependence on Serving Distance $r$

In our model, when the serving distance increases, the signal power received at the typical receiver decreases, while interference remains the same. Hence the SIR and $P_R$ are decreased. Figure 2.4 shows this effect.

### 2.3.4 Dependence on Medium Access Probability

When the medium access probability of interfering nodes ($p$) increases while the medium access probability of the typical node remains the same, the effective density of active interfering nodes ($p\lambda$) increases thus increasing the interference. Hence $P_R$ decreases, as shown in Figure 2.5. Also, when the medium access probability of typical node ($p'$) increases, $P_R$ increases. This is because the SIR distribution remains the same, whereas the typical transmitter transmits more often, thus increasing the rate.

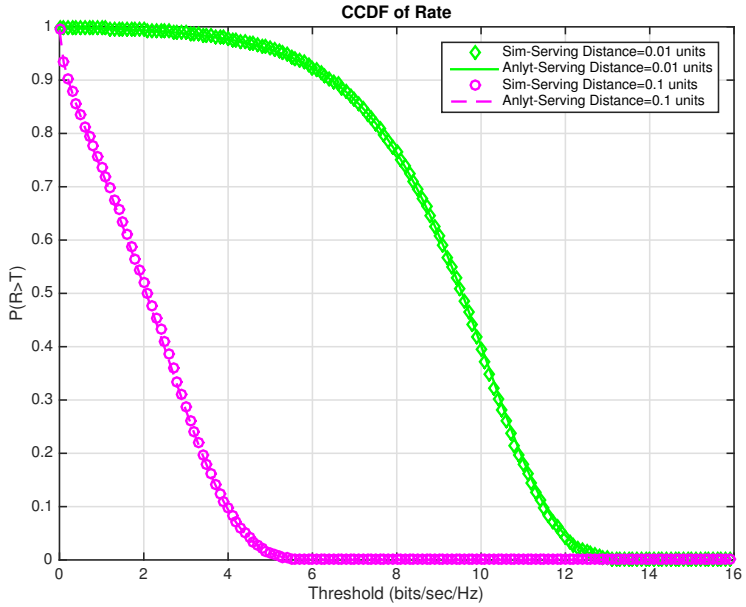


Figure 2.4: Dependence of rate on serving distance - Simulation vs Analysis. $P_R$ decreases with increase in $\alpha$.

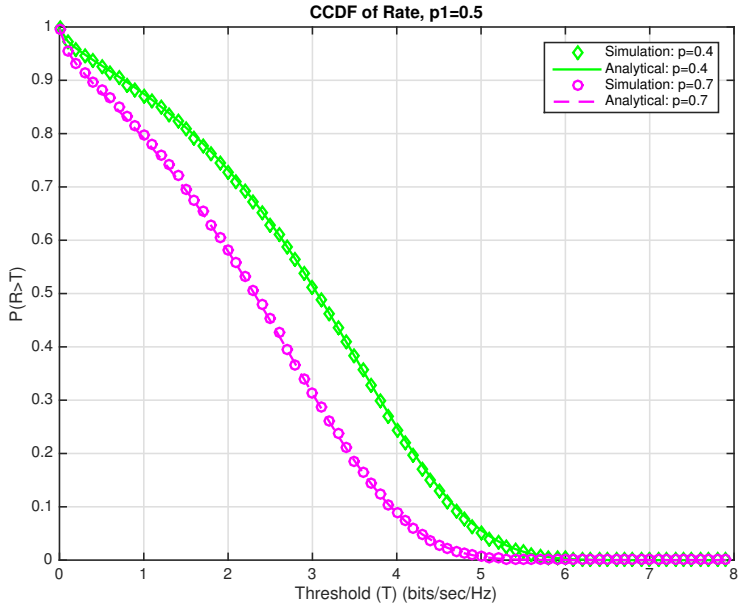


Figure 2.5: Dependence of rate on medium access probability of interfering nodes - Simulation vs Analysis. $P_R$ increases with increase in $p$.

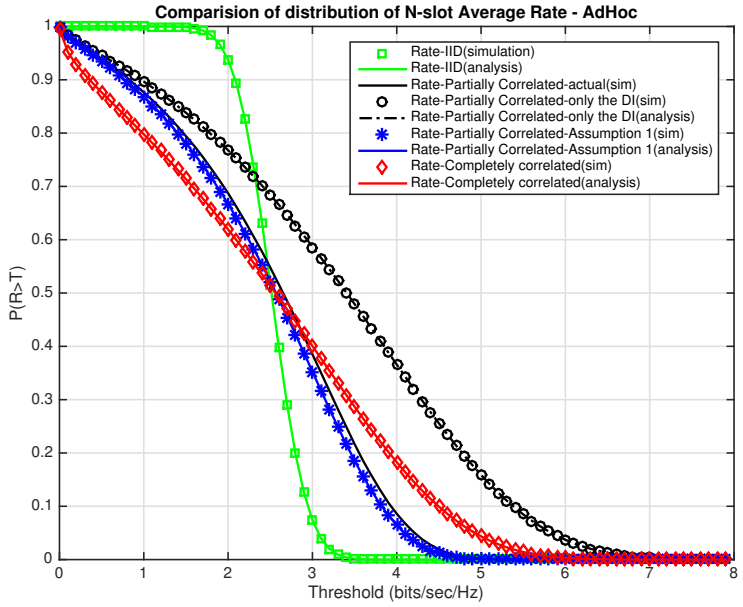


Figure 2.6: Simulation and Analytical results for $N$-slot average rate distribution in an ad hoc network - completely correlated rate, i.i.d. rate, and partially correlated rate.

Comparing the three cases in Figure 2.6, we observe that the CCDF of the $N$-slot average rate exhibits migh higher variance when the rates across time slots are completely correlated compared to the i.i.d. case. The partially correlated case lies in between these two extreme cases. In the plot, we have also included simulation and analytical results for approximating partially correlated rate using only the DI (Recall that Assumption 1 accounts for the DI and the mean interference caused by all other interferers given the DI distance). As can be observed, Assumption 1 produces a much more accurate approximation than considering only the DI. Also, since we used CLT, the approximation is tighter when we consider more time slots for our average rate metric.

## 2.4 Summary

In this chapter we characterized the $N$-slot average rate achievable by a typical node in an ad hoc network when the nodes are distributed according to a spatially homogenous PPP with a fixed serving distance. We derived analytical expressions for the distribution of the proposed $N$-slot average rate metric using two methods of approximation and discussed the relationship between this metric and various parameters associated with our model. We also covered three key scenarios of network mobility in our analysis. In the next chapter, we will perform this analysis for the downlink cellular network.

# Chapter 3

# Average Rate over Finite Time Slots in Downlink Cellular Network

While cellular networks have been traditionally modeled using deterministic grid models [30], a more recent way of modeling them is by using random spatial models, most often using homogeneous PPPs. Even though some early works in this area, e.g., see [31], were done almost two decades back, this approach gained popularity relatively recently. Interested readers are advised to refer to [10, 11, 32, 33] for more detailed exposition of the prior art in this area. Due to the existence of these books, surveys, and tutorials, we will keep this discussion focused by discussing the most relevant prior art.

On the same lines as the previous chapter, we derive expressions for the proposed $N$-slot average rate metric in a downlink cellular network where the locations of base stations (BS) are spatially distributed according to a homogenous PPP. In our model, a typical receiver (user) associates with its nearest base station and all other base stations act as interferers to the user. More details are provided next.

## 3.1 PPP-based Model for Downlink Cellular Network

As is usually the case in stochastic geometry-based approaches for modeling cellular networks, we assume that the BS locations are modeled using a homogeneous PPP $\Phi_k$ with density $\lambda$. The user locations are assumed to be independent of the BS locations. The downlink analysis will be performed for the reference receiver located at the origin. For cell selection, we assume that this user remains connected to the closest BS across all the time slots considered. Each interferer is active with a probability $\hat{p}$, known as the activity factor [34], in each time slot.

As was the case in the previous chapter, we model the path loss for a wireless link between a BS located at $x$ and the user as: $l(\|x\|) = \|x\|^{-\alpha}$ where $\alpha > 2$ is the path loss exponent, and $\|x\|$ represents the Euclidean distance between point $x$ and the origin. We assume Rayleigh fading channels and that the fading gains are i.i.d. across all communication links in all time slots. The fading gain between a BS at $X_{j_{\tilde{\Phi}_k}}$ and the receiver at the origin in time slot $k$ is represented by $h_{j,k} \sim \exp(1)$. Without loss of generality, we assume that the transmit power of all the BSs is unity in all time slots. To be consistent with the notation used in the previous chapter, we denote the locations of active BSs (including the one serving the typical user at the origin) in time slot $k$ by $\tilde{\Phi}_k$. The location of the serving BS will be denoted by $X_{0_{\tilde{\Phi}_k}}$.

As discussed in Chapter 2, we again characterize our metric in the following three cases: completely correlated rate, i.i.d. rate, and partially correlated rate. Please refer to Chapter 2 for the description of the three cases.

### Distance to the Closest BS

The distance from the user to the nearest BS is represented by the random variable $Y_1$, where $Y_1 = \|X_{0_{\tilde{\Phi}_k}}\|$ in our cellular network model. Using the void probability of the homogeneous PPP, the CCDF of $Y_1$ can be expressed as [5]:

$$Pr\left(Y_1 > x\right) = \exp\left(-\lambda\pi x^2\right). \tag{3.1}$$

Using the complementary CDF, the pdf function can be found:

$$f_{Y_1}(x) = 2\pi\lambda x \exp\left(-\lambda\pi x^2\right). \tag{3.2}$$

## 3.2 $N$-slot Average Rate Distribution in Cellular Downlink

In our network model, the maximum achievable rate of a user per unit bandwidth in bits/sec/Hz in time slot k is given by:

$$R_k = \log_2\left(1 + \frac{h_{0,k}\, l(Y_1)}{\sum_{X_{j_{\tilde{\Phi}_k}} \in \tilde{\Phi}_k, j\neq 0} h_{j,k}\, l(\|X_{j_{\tilde{\Phi}_k}}\|)}\right), k \geq 1. \tag{3.3}$$

We denote the probability that $N$-slot average rate is larger than some threshold $T$ (bits/sec/Hz) i.e. $Pr(\tilde{R} > T)$ by $P_R$ which is given by

$$P_R = Pr\left(\frac{\sum_{k=1}^{N} R_k}{N} > T\right) \tag{3.4}$$

$$= Pr\left(\frac{\sum_{k=1}^{N} \log_2\left(1 + \frac{h_{0,k}\, l(Y_1)}{\sum_{X_{j_{\tilde{\Phi}_k}} \in \tilde{\Phi}_k, j\neq 0} h_{j,k}\, l(\|X_{j_{\tilde{\Phi}_k}}\|)}\right)}{N} > T\right). \tag{3.5}$$

Before deriving the distribution of $N$-slot average rate, we state the downlink coverage probability for this setup, which was derived in [12] and is a fairly well-known result by now.

**Lemma 2.** Under Rayleigh Fading, the coverage probability of a typical BS in an interference-

limited downlink cellular network is

$$p_c(\hat{p}, \lambda, T) = \int_0^\infty \exp\left(-\pi\lambda r^2\right) \mathcal{L}_I\left(\mu T r^\alpha\right) 2\pi\lambda r \mathrm{d}r \tag{3.6}$$

where $\mathcal{L}_I(.)$ represents the Laplace transform of interference $I$ evaluated at its argument conditioned on the distance to the serving BS (nearest) from the origin and is given as follows:

$$\mathcal{L}_I\left(\mu T r^\alpha\right) = \exp\left(-\pi r^2 \hat{p}\lambda\, \rho(T, \alpha)\right) \tag{3.7}$$

where $\rho(T, \alpha) = T^{2/\alpha} \int_{T^{-2/\alpha}}^\infty \frac{1}{1 + u^{(\alpha/2)}} \mathrm{d}u$. For proof, see [12].

In (3.7), we consider thinning of interference corresponding to the activity factor $\hat{p}$. By substituting (3.7) in (3.6), and using variable transformation $r^2 \to v$, we get the simplified expression for coverage probability as follows.

$$p_c(T, \alpha, \hat{p}) = \frac{1}{1 + \hat{p}\rho(T, \alpha)}. \tag{3.8}$$

We use the above result to derive an expression for the distribution of average rate.

### 3.2.1 Rate in the Completely Correlated Case

When rate across time slots is completely correlated, say $R_k = R$, it means that the BS locations and interference remain the same across $N$ time slots. In this case, the CCDF of $N$-slot average rate, $P_R$ equals the CCDF of rate in each individual time slot:

$$\begin{aligned} P_R &= Pr\left(R > T\right) && (3.9)\\ &= Pr\left(R_k > T\right) && (3.10)\\ &= Pr\left(\log_2(1 + \mathrm{SIR_k}) > T\right) && (3.11)\\ &= Pr\left(\mathrm{SIR_k} > 2^T - 1\right) && (3.12) \end{aligned}$$

$$= p_c(2^T - 1, \alpha, \hat{p}) \tag{3.13}$$

$$= \frac{1}{1 + \hat{p}\rho(2^T - 1, \alpha)} \tag{3.14}$$

where the last equation follows from (3.8).

### 3.2.2 Rate in the i.i.d. Case

This is the scenario in which the locations of the BSs and the channel fading in each link are i.i.d. across time slots (as discussed already, this extreme case corresponds to a *high mobility* scenario). We derive a mathematical expression for $P_R$ by using a similar approach (approximation by CLT) as was used in Section 2.2. We evaluate the mean and second moment of $R_k$ (denoted by $\mu_{R_k}$ and $M_{R_k}$, respectively), and thereby variance of $\tilde{R}$ (denoted by $\sigma^2_{\tilde{R}}$) as follows.

Since $R_k$ are i.i.d. random variables, the mean of $\tilde{R}$ is: $E[\tilde{R}] = E[R_k]$. Since, rate is a non-negative random variable, mean of $R_k$ can be written as:

$$\mathbb{E}[R_k] = \int_0^\infty Pr\left(\log_2(1 + \mathrm{SIR}_k) > x\right) \mathrm{d}x \tag{3.15}$$

$$= \int_0^\infty \frac{1}{1 + \hat{p}\rho(2^x - 1, \alpha)} \mathrm{d}x \tag{3.16}$$

where the last equation follows from (3.14).
Similarly, the second moment of each individual $R_k$ is given by:

$$E[R_k^2] = \int_0^\infty Pr\left((\log_2(1 + \mathrm{SIR}_k))^2 > x\right) \mathrm{d}x \tag{3.17}$$

$$= \int_0^\infty Pr\left(\log_2(1 + \mathrm{SIR}_k) > \sqrt{x}\right) \mathrm{d}x \tag{3.18}$$

$$= \int_0^\infty Pr\left(\mathrm{SIR}_k > 2^{\sqrt{x}} - 1\right) \mathrm{d}x \tag{3.19}$$

$$= \int_0^\infty \frac{1}{1+\hat{p}\rho\left(2^{\sqrt{x}}-1,\alpha\right)}\mathrm{d}x \tag{3.20}$$

where the last equation follows from (3.14).

Since $R_k$ are i.i.d., variance of $\tilde{R}$ is calculated as follows:

$$\sigma^2_{\tilde{R}} = \frac{M_{R_k} - \mu^2_{\tilde{R}}}{N}. \tag{3.21}$$

Using the mean and variance, we derive the desired CCDF of $\tilde{R}$ as

$$P_R = \varphi\left(\frac{x-(\mu_{\tilde{R}})}{\sqrt{\frac{M_{R_k}-(\mu_{\tilde{R}})^2}{N}}}\right) \tag{3.22}$$

where the function $\varphi$ is the CCDF of a standard Normal random variable.

### 3.2.3 Rate in the Partially Correlated Case

The locations of BSs in this scenario do not change across $N$ time slots, while the channel fading gains are i.i.d. across links and time slots. In our downlink cellular model, the serving distance $Y_1$ is a random variable. $\tilde{\Phi}$ represents the locations of active BSs and is independent of time slots in the partially correlated case of rate. Conditioning on $Y_1$ and using Assumption 1, we derive the conditional CCDF for $N$-slot average rate by using similar approach (approximation by CLT) as in Section 2.2. Then we decondition with respect to $Y_1$ and the distance of the DI ($D$) using their joint density function to derive a mathematical expression for $P_R$.

**Lemma 3.** In $\tilde{\Phi}$, the joint pdf of distances of the closest and next closest point to the origin, denoted by $Y_1$ and $D$ respectively, is given as:

$$f_{Y_1,D}(y_1,d_1) = \hat{p}\, y_1 d_1 (2\pi\lambda)^2 \exp\left(-\lambda\pi y_1^2(1-\hat{p})\right)\exp\left(-\hat{p}\lambda\pi d_1^2\right) \tag{3.23}$$

where $\lambda$ represents the density of the point process and $\hat{p}$ is the activity factor of the interfering BSs. See [29, 35] for a proof of this lemma.

The expression for $N$-slot average rate distribution for partially correlated rate is given by:

$$P_R = Pr\left( \frac{\sum_{k=1}^{N} \log_2\left(1 + \frac{h_{0,k} l(Y_1)}{I_{\tilde{\Phi},k}}\right)}{N} > T \right) \tag{3.24}$$

where interference term is $I_{\tilde{\Phi},k} = \sum_{X_j \in \tilde{\Phi},\, j \neq 0} h_{j,k} l(\|X_j\|)$. In this partially correlated case of rate, we denote interference by $I_{\tilde{\Phi},k}$ (instead of $I_{\tilde{\Phi}_k}$) as the distribution of node locations is the same across all time slots.

After jointly conditioning on the distances to serving BS and DI, the individual interferences and hence the individual rates $R_k$ become i.i.d. and thus we can apply the CLT to conditioned $\tilde{R}$ for large enough $N$. After conditioning, the interference $I_{\tilde{\Phi},k}$ is given by (2.50).

$$\hat{I}_{\tilde{\Phi},k} = h_{1,k} {d_1}^{-\alpha} + \frac{2\hat{p}\pi\lambda}{\alpha - 2} {d_1}^{2-\alpha} \tag{3.25}$$

Using similar approach to derive the conditional CCDF of individual rate as in section 2.2 (using Assumption 1), we get the following expression identical to (2.65):

$$Pr\left(\hat{R}_k > x \,|\, D = d_1, Y_1 = y_1\right) = \frac{\exp\left\{ -\left(2^{x/\hat{p}} - 1\right) \frac{2\hat{p}\pi\lambda y_1^2}{\alpha - 2} \left(\frac{d_1}{y_1}\right)^{2-\alpha} \right\}}{\left(2^{x/\hat{p}} - 1\right) \left(\frac{d_1}{y_1}\right)^{-\alpha} + 1} \tag{3.26}$$

After joint conditioning, $\{R_k\}$ become i.i.d. random variables and the conditional mean of $\tilde{R}$ is: $E[\tilde{R} \,|\, D = d_1, Y_1 = y_1] = E[R_k \,|\, D = d_1, Y_1 = y_1]$

Using (3.26), the conditional first moment ($\mu_{R_k|D=d_1,Y_1=y_1}$) and conditional second moment ($M_{R_k|D=d_1,Y_1=y_1}$) of $R_k$ are given as:

$$\mu_{R_k|Y_1=y_1,D=d_1} = \int_0^\infty \frac{\exp\left\{-\left(2^{x/\hat{p}}-1\right)\frac{2\hat{p}\pi\lambda y_1^2}{\alpha-2}\left(\frac{d_1}{y_1}\right)^{2-\alpha}\right\}}{\left(2^{x/\hat{p}}-1\right)\left(\frac{d_1}{y_1}\right)^{-\alpha}+1}\,\mathrm{d}x \tag{3.27}$$

$$M_{R_k|Y_1=y_1,D=d_1} = \int_0^\infty \frac{\exp\left\{\left(1-2^{\sqrt{x}/\hat{p}}\right)\frac{2\hat{p}\pi\lambda y_1^2}{\alpha-2}\left(\frac{d_1}{y_1}\right)^{2-\alpha}\right\}}{\left(2^{\sqrt{x}/\hat{p}}-1\right)\left(\frac{d_1}{y_1}\right)^{-\alpha}+1}\mathrm{d}x \tag{3.28}$$

We then evaluate the conditional CCDF of rate $\bar{F}(\tilde{R}|y_1,d_1)$ using the following expression.

$$\bar{F}(\tilde{R}|y_1,d_1) = \varphi\left(\frac{x-\left(\mu_{R_k|y_1,d_1}\right)}{\sqrt{\frac{M_{R_k|y_1,d_1}-\left(\mu_{R_k|y_1,d_1}\right)^2}{N}}}\right) \tag{3.29}$$

where the function $\varphi$ is the CCDF of a standard Normal random variable. Now we derive the desired CCDF of $N$-slot average rate (represented as $P_R$) by deconditioning using the joint pdf (Lemma 3) of serving distance ($Y_1$) and the DI distance ($D$) as follows:

$$P_R = \int_0^\infty\int_{y_1}^\infty \bar{F}(\tilde{R}|y_1,d_1) f_{Y_1,D}(y_1,d_1)\,\mathrm{d}y_1\,\mathrm{d}d_1 \tag{3.30}$$

$$= \int_0^\infty\int_{y_1}^\infty \varphi\left(\frac{x-\left(\mu_{R_k|y_1,d_1}\right)}{\sqrt{\frac{M_{R_k|y_1,d_1}-\left(\mu_{R_k|y_1,d_1}\right)^2}{N}}}\right) f_{Y_1,D}(y_1,d_1)\,\mathrm{d}y_1\,\mathrm{d}d_1 \tag{3.31}$$

$$= \int_0^\infty\int_{y_1}^\infty \varphi\left(\frac{x-\left(\mu_{R_k|y_1,d_1}\right)}{\sqrt{\frac{M_{R_k|y_1,d_1}-\left(\mu_{R_k|y_1,d_1}\right)^2}{N}}}\right) \hat{p}y_1d_1(2\pi\lambda)^2 e^{\left(-\lambda\pi y_1^2(1-\hat{p})-\hat{p}\lambda\pi d_1^2\right)}\mathrm{d}y_1\mathrm{d}d_1 \tag{3.32}$$

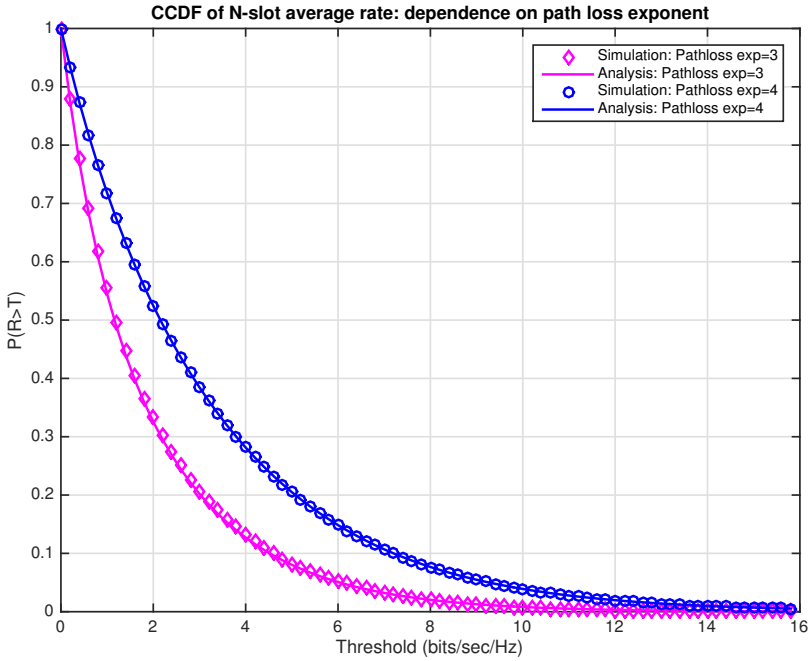


Figure 3.1: Dependence of rate on path-loss exponent - Simulation vs Analysis. $P_R$ increases with increase in $\alpha$

## 3.3 Results and Discussion

In this section we present numerical results and validate various approximations made in the analysis. Our results demonstrate that probability $P_R$ increases with increase in the path-loss exponent, decreases with increase in the activity factor, and remains the same with change in the density of BSs.

### 3.3.1 Dependence on Path-loss Exponent $\alpha$

When the path-loss exponent increases, the signal power at the typical receiver from its associated BS decreases. However, the signal powers from every interfering BS are also decreased. Overall, interference decreases more than the signal power and hence SIR increases, thus leading to higher $P_R$. Figure 3.1 shows this effect.

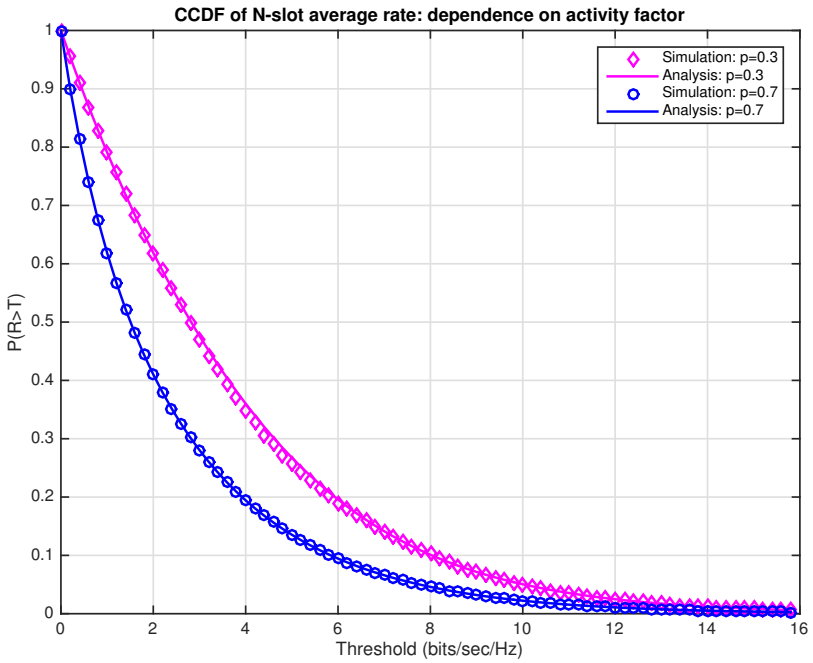


Figure 3.2: Dependence of rate on activity factor of BSs - Simulation vs Analysis. $P_R$ decreases with increase in $\hat{p}$

### 3.3.2 Dependence on Activity Factor $\hat{p}$

In our cellular network model, the user always remains connected to its closest BS across the time slots, while the interfering BSs transmit and mute with probability $\hat{p}$ and $1-\hat{p}$ respectively. Hence, when the activity factor ($\hat{p}$) increases, the effective density of active interfering BSs ($\hat{p}\lambda$) increases thus increasing the interference. Hence $P_R$ decreases, as shown in Figure 3.2.

### 3.3.3 Dependence on Density of Base Stations $\lambda$

When the density of BSs increases, the nearest BS to the typical user will be closer than before and thus the desired signal power increases. However, increased density of interfering BSs will cause higher interference. Overall, these effects counteract each other leading to same SIR and thus same $P_R$. Figure 3.3 shows this effect.

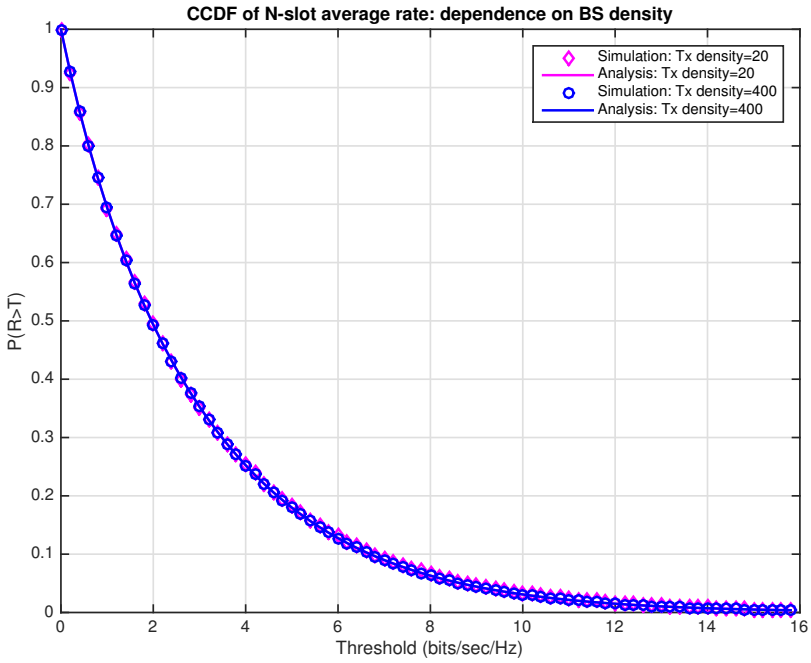


Figure 3.3: Dependence of rate on density of BSs - Simulation vs Analysis. $P_R$ remains the same with change in $\lambda$

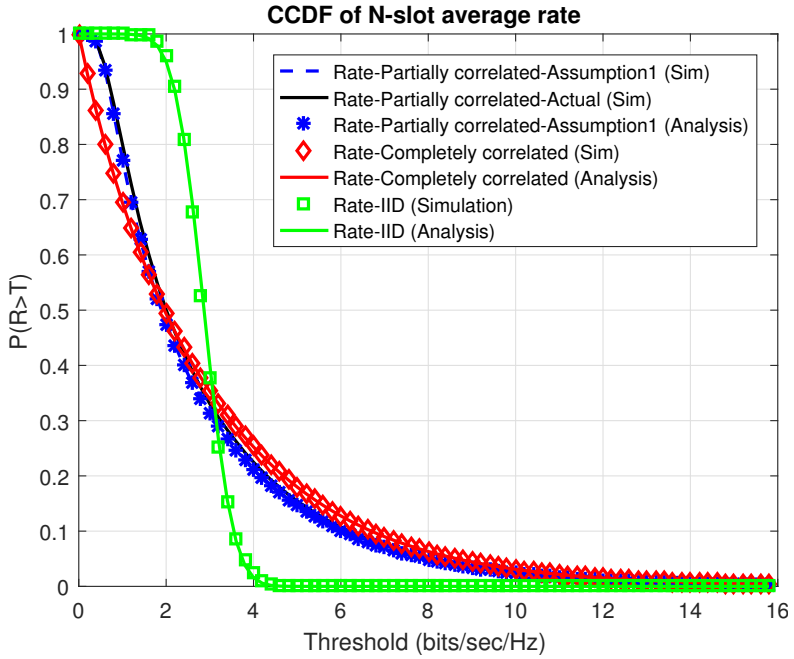


Figure 3.4: Simulation and Analytical results for $N$-slot average rate distribution in cellular downlink - completely correlated rate, i.i.d. rate, and partially correlated rate

Comparing the three cases in Figure 3.4, we can observe a similar result as in ad hoc network: When rate across time slots is highly correlated, the CCDF of $N$-slot average rate exhibits much higher variance. As can be observed, Assumption 1 produces an accurate approximation in our cellular downlink model. Also, since we used CLT, the approximation is tighter when we consider more time slots for our average rate metric.

## 3.4 Summary

In this chapter we characterized the $N$-slot average rate achievable by a typical user in the downlink of a cellular network when the BSs are distributed in 2-dimensional space according to a spatially homogenous PPP. Under nearest BS connectivity model, we derived analytical expressions for the distribution of $N$-slot average rate using DI assumption and CLT approximation which yielded accurate results and discussed the relationship between this metric and various parameters associated with our model. We also covered three key scenarios of network mobility in our analysis.

# Chapter 4

# Conclusion

## 4.1 Summary

In this thesis, we proposed and analyzed a new rate metric, termed the $N$-slot average rate, for both ad hoc and cellular networks. The proposed metric generalizes the notion of instantaneous and ergodic rates by allowing the computation of average rate over a given number, say $N$, of time slots. While the mathematical form of the proposed metric makes it difficult to derive its exact distribution, we employ suitable approximations to derive tractable expressions, which are numerically shown to be remarkably close to the true distribution. We performed our analysis for three different mobility scenarios, which result in vastly different assumptions on various random variables involved in the analysis. The key contributions of this thesis are summarized next.

In Chapter 2, we characterized $N$-slot average rate achievable by a typical node in ad hoc network. We considered Poisson bipolar MANET with a fixed serving distance between a transmitter and its paired receiver. Having propounded the intractability of the method involving Fourier inversion of product of characteristic functions of rates in each time slot, we take an alternate approach employing simple yet meaningful approximations (DI and CLT)

which yielded accurate results. We discussed the impact of various system parameters on the distribution of our metric which is crucial to understand the network performance. Our analysis showed that when the rate across time slots is highly correlated, the distribution of $N$-slot average rate exhibits higher variance in bipolar MANETs. The significance of this observation is relatable to the practical case of understanding the Quality-of-Experience (QoE) for user-centric services provided in such networks.

In Chapter 3, we characterized our metric $N$-slot average rate in the cellular downlink. We considered a homogeneous PPP model for the BS locations with a given activity factor and nearest BS association policy. As in Chapter 2, we use appropriate approximations to derive the distribution of the proposed metric in this case under three different mobility scenarios of interest. The accuracy and simplicity of our approximate expressions make them of practical interest to the cellular network designers. We also discussed the relationship between our metric and system parameters, and again, our analysis showed that the variance of the distribution of our metric is more when the rate across time slots is highly correlated. This key insight helps us in understanding the user's QoE for cellular services, for example, Voice over LTE (VoLTE).

## 4.2 Future Directions

In this section, we discuss two possible directions for future research.

### 4.2.1 Characterization of the Average Rate Achievable in Heterogeneous Cellular Networks over Finite Time Slots

The analysis presented in Chapter 3 can be extended to characterize $N$-slot average rate in heterogeneous cellular networks consisting of $K$ overlaid tiers of BSs (modeling different types of BSs, such as macro, pico, micro, and femtocells). As discussed in [13], we can

assume $K$ different types of BSs, each modeled by an independent PPP. Then the downlink analysis can be performed on the same lines as in Chapter 3. More sophisticated models based on Poisson cluster processes, such as in [36–39] can also be used. This will significantly enhance the state-of-the-art in heterogeneous cellular networks, where the analysis is usually focused on spatially averaged throughput without accounting for the temporal aspect, which is captured very well by the proposed metric.

### 4.2.2 Buffer Dynamcs in an Ad Hoc Network

Another worthwhile extension is to incorporate temporal dynamics explicitly in the models. For instance, in video streaming and other such applications, we are particularly interested in the temporal evolution of the number of bits in the buffer. The buffer can be thought to fill at the rate proportional to the transmission rate and empty at a constant utilization rate (function of the application). The evolution of the number of bits in the buffer can therefore be modeled as a continuous time Markov chain (more specifically, birth-death process). For this Markov chain, mean hitting time [40] to state 0 will give the mean time until the first disruption in the video stream. Such estimates are very useful for system designers.

# Bibliography


[1] D. B. Taylor, H. S. Dhillon, T. D. Novlan, and J. G. Andrews, "Pairwise interaction processes for modeling cellular network topology," in *Proc., IEEE Global Commun. Conf. (GLOBECOM)*, Dec. 2012, pp. 4524–4529.

[2] A. Guo and M. Haenggi, "Spatial stochastic models and metrics for the structure of base stations in cellular networks," *IEEE Trans. on Wireless Commun.*, vol. 12, no. 11, pp. 5800 – 5812, Nov. 2013.

[3] C.-H. Lee, C.-Y. Shih, and Y.-S. Chen, "Stochastic geometry based models for modeling cellular networks in urban areas," *Wireless Networks*, vol. 19, no. 6, pp. 1063–1072, 2013.

[4] S. N. Chiu, D. Stoyan, W. S. Kendall, and J. Mecke, *Stochastic Geometry and its Applications*, 3rd ed. New York: John Wiley and Sons, 2013.

[5] M. Haenggi, *Stochastic Geometry for Wireless Networks*. Cambridge University Press, 2012.

[6] F. Baccelli and B. Blaszczyszyn, *Stochastic Geometry and Wireless networks, Volume 1- Theory*. NOW: Foundations and Trends in Networking, 2009.

[7] M. Z. Win, P. C. Pinto, and L. A. Shepp, "A mathematical theory of network interference and its applications," *Proceedings of the IEEE*, vol. 97, no. 2, pp. 205–230, Feb 2009.

[8] M. Haenggi, J. G. Andrews, F. Baccelli, O. Dousse, and M. Franceschetti, "Stochastic geometry and random graphs for the analysis and design of wireless networks," *IEEE Journal on Sel. Areas in Commun.*, vol. 27, no. 7, pp. 1029–1046, Sep. 2009.

[9] H. Elsawy, E. Hossain, and M. Haenggi, "Stochastic geometry for modeling, analysis, and design of multi-tier and cognitive cellular wireless networks: A survey," *IEEE Commun. Surveys and Tutorials*, vol. 15, no. 3, pp. 996–1019, 3th quarter 2013.

[10] J. G. Andrews, A. K. Gupta, and H. S. Dhillon, "A primer on cellular network analysis using stochastic geometry," *arXiv preprint*, 2016, available online: arxiv.org/abs/1604.03183.

[11] H. ElSawy, A. Sultan-Salem, M. S. Alouini, and M. Z. Win, "Modeling and analysis of cellular networks using stochastic geometry: A tutorial," *IEEE Communications Surveys Tutorials*, vol. 19, no. 1, pp. 167–203, Firstquarter 2017.

[12] J. G. Andrews, F. Baccelli, and R. K. Ganti, "A tractable approach to coverage and rate in cellular networks," *IEEE Transactions on Communications*, vol. 59, no. 11, pp. 3122–3134, 2011.

[13] H. S. Dhillon, R. K. Ganti, F. Baccelli, and J. G. Andrews, "Modeling and analysis of $K$-tier downlink heterogeneous cellular networks," *IEEE Journal on Sel. Areas in Commun.*, vol. 30, no. 3, pp. 550–560, Apr. 2012.

[14] F. Baccelli, B. Blaszczyszyn, and P. Muhlethaler, "Stochastic analysis of spatial and opportunistic aloha," *IEEE Journal on Selected Areas in Communications*, vol. 27, no. 7, pp. 1105–1119, 2009.

[15] K. Huang, "Spatial throughput of mobile ad hoc networks powered by energy harvesting," *IEEE Transactions on Information Theory*, vol. 59, no. 11, pp. 7597–7612, 2013.

[16] X. Zhang and M. Haenggi, "The aggregate throughput in random wireless networks with successive interference cancellation," in *2013 IEEE International Symposium on Information Theory*, 2013, pp. 251–255.

[17] C. H. Liu and J. G. Andrews, "Ergodic transmission capacity of wireless ad hoc networks with interference management," *IEEE Transactions on Wireless Communications*, vol. 11, no. 6, pp. 2136–2147, 2012.

[18] Y. George, I. Bergel, and E. Zehavi, "The ergodic rate density of aloha wireless ad-hoc networks," *IEEE Transactions on Wireless Communications*, vol. 12, no. 12, pp. 6340–6351, 2013.

[19] S. Weber, J. G. Andrews, and N. Jindal, "The effect of fading, channel inversion, and threshold scheduling on ad hoc networks," *IEEE Transactions on Information Theory*, vol. 53, no. 11, pp. 4127–4149, 2007.

[20] J. Andrews, A. Ghosh, and R. Muhamed, *Fundamentals of WiMAX: Understanding Broadband Wireless Networking*, ser. Prentice Hall Communications Engineering and Emerging Technologies Series from Ted Rappaport. Pearson Education, 2007.

[21] J. Schloemann, H. S. Dhillon, and R. M. Buehrer, "Toward a tractable analysis of localization fundamentals in cellular networks," *IEEE Transactions on Wireless Communications*, vol. 15, no. 3, pp. 1768–1782, 2016.

[22] T. Bhandari, H. S. Dhillon, and R. M. Buehrer, "The impact of proximate base station measurements on localizability in cellular systems," in *Proc., IEEE SPAWC*, Edinburgh, UK, Jul. 2016.

[23] V. V. Chetlur and H. S. Dhillon, "Downlink coverage probability in a finite network of unmanned aerial vehicle (UAV) base stations," in *Proc., IEEE SPAWC*, Edinburgh, UK, Jul. 2016.

[24] ——, "Downlink coverage analysis for a finite 3D wireless network of unmanned aerial vehicles," arXiv preprint, Oct. 2016, available online: arxiv.org/abs/1604.03183.

[25] M. Haenggi, "The meta distribution of the SIR in poisson bipolar and cellular networks," *IEEE Transactions on Wireless Communications*, vol. 15, no. 4, pp. 2577–2589, 2016.

[26] M. K. Hanawal, E. Altman, and F. Baccelli, "Stochastic geometry based medium access games in wireless ad hoc networks," *IEEE Journal on Selected Areas in Communications*, vol. 30, no. 11, pp. 2146–2157, 2012.

[27] J. G. Andrews, R. K. Ganti, M. Haenggi, N. Jindal, and S. Weber, "A primer on spatial modeling and analysis in wireless networks," *IEEE Communications Magazine*, vol. 48, no. 11, pp. 156–163, 2010.

[28] Y. Zhong, W. Zhang, and M. Haenggi, "Managing interference correlation through random medium access," *IEEE Transactions on Wireless Communications*, vol. 13, no. 2, pp. 928–941, 2014.

[29] M. Haenggi, "On distances in uniformly random networks," *IEEE Transactions on Information Theory*, vol. 51, no. 10, pp. 3584–3586, 2005.

[30] T. S. Rappaport, *Wireless Communications: Principles and Practice*, ser. Prentice Hall communications engineering and emerging technologies series, 2009.

[31] F. Baccelli, M. Klein, M. Lebourges, and S. Zuyev, "Stochastic geometry and architecture of communication networks," *Telecommunication Systems*, vol. 7, no. 1, pp. 209–227, 1997.

[32] H. S. Dhillon, "Fundamentals of heterogeneous cellular networks," Ph.D. dissertation, The University of Texas at Austin, TX, USA, Dec. 2013.

[33] S. Mukherjee, *Analytical Modeling of Heterogeneous Cellular Networks: Geometry, Coverage, and Capacity*. New York: Cambridge University Press, 2014.

[34] H. S. Dhillon, R. K. Ganti, and J. G. Andrews, "Load-aware modeling and analysis of heterogeneous cellular networks," *IEEE Trans. on Wireless Commun.*, vol. 12, no. 4, pp. 1666 – 1677, Apr. 2013.

[35] ——, "Modeling non-uniform UE distributions in downlink cellular networks," *IEEE Wireless Communications Letters*, vol. 2, no. 3, pp. 339–342, 2013.

[36] C. Saha, M. Afshang, and H. S. Dhillon, "Enriched $K$-tier HetNet model to enable the analysis of user-centric small cell deployments," *IEEE Trans. on Wireless Commun.*, vol. 16, no. 3, pp. 1593–1608, Mar. 2017.

[37] C. Saha and H. S. Dhillon, "Downlink coverage probability of K-tier hetnets with general non-uniform user distributions," in *Proc., IEEE Intl. Conf. on Commun. (ICC)*, Kuala Lumpur, Malaysia, May 2016.

[38] C. Saha, M. Afshang, and H. S. Dhillon, "Poisson cluster process: Bridging the gap between PPP and 3GPP hetnet models," in *Proc., Information Theory and its Applications (ITA)*, San Diego, CA, Feb. 2017.

[39] M. Afshang and H. S. Dhillon, "Poisson cluster process based analysis of HetNets with correlated user and base station locations," arXiv:1612.07285, 2016.

[40] H. S. Dhillon, Y. Li, P. Nuggehalli, Z. Pi, and J. G. Andrews, "Fundamentals of heterogeneous cellular networks with energy harvesting," *IEEE Transactions on Wireless Communications*, vol. 13, no. 5, pp. 2782–2797, 2014.